Materials Research Proceedings 41 (2024) 257-263 https://doi.org/10.21741/9781644903131-29

Laser metal deposition of NbTaTiV refractory high entropy alloy

BARTH Eric[1,a *] and HOR Anis[1,b]

[1]Espace Clément Ader, 3 Rue Caroline Aigle d'Aigle, 31400 Toulouse, France

[a]eric.barth@isae-supaero.fr, [b]anis.hor@isae-supaero.fr

Keywords: Additive Manufacturing, Laser Metal Deposition, High Temperature, Microstructure, Complex Concentrated Alloys

Abstract. A mixture of Ti, V, Nb and Ta elemental powders was used to print an equimolar Refractory High Entropy Alloy NbTaTiV. Single beads and wall structures were printed on Ti-6Al-4V substrates. The samples were then cut to analyze their cross-section and composition. The samples present a large proportion of non-melted Ta particles, due to the low max power of the used laser (500W) and of the high melting-point of Ta. It was found that using a two-step deposition process (deposition, followed by a powder-less re-melting pass) could allow to homogenize the samples and melt said Ta particles. Moreover, the authors report difficulty to control the composition of the samples due to the very different physical properties of the different elements composing the alloy, with a preferential deposition of Ta.

Introduction

The concept "High Entropy Alloys (HEA)" was first theorized by Yeh et al. [1] and Cantor et al. [2] in 2004, as a novel way to design alloys by mixing elements in equimolar or close to equimolar proportions. Since then, a sub-category was introduced by Senkov et al. [3]: Refractory High Entropy Alloys (RHEA), made of refractory elements such as Ta, W and Mo. These alloys have immediately attracted high interest, due to their exceptional resistance at extreme temperatures (over 1 600°C) [4], [5]. However, several drawbacks hinder their potential applications. Most notably, as of now, the majority of RHEA is extremely brittle at room temperature [3], [6]. Moreover, their high melting points and complex composition makes it challenging to obtain homogeneous ingots through conventional casting processes [7]. Therefore, using a process with a small size melt-pool and a fast cooling process could help to obtain homogeneous samples. Hence the recent interest in building these materials through additive manufacturing processes, more specifically powder based deposition processes, such as Laser Metal Deposition (LMD). On top of inducing the small melt pools and fast cooling rates that can help to obtain homogeneous samples, this process can be used to build sample from a mixture of elemental powders, whose chemical composition can be modified *in-situ* to generate a composition gradient. This gradient can be used in functional parts, to deposit the highly expensive elements only where they are needed, but also to allow for a high-throughput analysis of all composition opened by the HEA conception paradigm shift. However, LMD requires a minimal level of ductility, as the fast cooling rates can generate residual stresses, which can result in high cracks density if the material is too brittle [6].

In 2018, Lee et al. proposed a new BCC RHEA, with both high resistance at elevated temperatures and good ductility at room temperatures [8], an equimolar mixture of Ti, V, Nb and Ta. This alloy system could be a promising candidate, as its ductility would allow it to be manufactured by additive processes. However, the large differences in the different elements' properties, such as melting temperature (1 668°C for Ti and 3 020°C for Ta) and density (4.51g/cm³ for Ti and 16.4g/cm³ for Ta) can lead to new challenges, even more so if one uses a mixture of pure elemental powder instead of pre-alloyed ones. These differences can lead to heterogeneities and to difficulties to achieve the desired sample's composition [6], [9].

This paper, therefore, offers to study the manufacturability of the NbTaTiV RHEA by LMD.

Material and method

Samples were manufactured using a mixture of high purity (99,9 %at) Ti, V, Nb and Ta elemental powders, manufactured by Metal Powder Tech International, with a 45-90 µm particle size. All powders were found to have good sphericity, except Ti powders, within which a number of particles had highly irregular shapes. The powders dimensions were within the desired margins, except for Ta which was found to have a large fraction of smaller particles.

In order to consider heterogeneous deposition efficiencies of the different elements, a non-equimolar $Ti_{25}V_{20}Nb_{20}Ta_{35}$ powder chemical composition was selected on the basis of the literature review [10], [11]. The mixing process was performed manually in a controlled environment.

The powder mixture was then poured in a powder hopper connected to a commercial BeAM Mobile, an LPBF additive manufacturing machine, equipped with a 5-axis deposition system, a 500W Nd:YAG laser and a sealed chamber, used in this study to manufacture the samples under Ar atmosphere.

20mm-long single tracks and 4-layers wall samples were then printed in an inert atmosphere (<1000ppm O_2) on a Ti-6Al-4V substrate using variable laser powers (P), printhead speed (V) and powder mass-flow ($\dot{m}$). The upper and lower limits of these parameters are reported in Table 1.

Table 1: Upper and lower limits of the manufacturing parameters

Laser Power [W]	Printhead speed [mm/min]	Powder mass-flow [g/min]
400 - 500	400 - 1200	3.5 – 7.3

As suggested by Dobbelstein et al. [6], some samples were manufactured using a 2-step deposition process. First, a conventional deposition step, followed by a second re-melting pass, without adding more powder (Fig. 1). This process is meant to ensure the melting of the high melting-temperature elements.

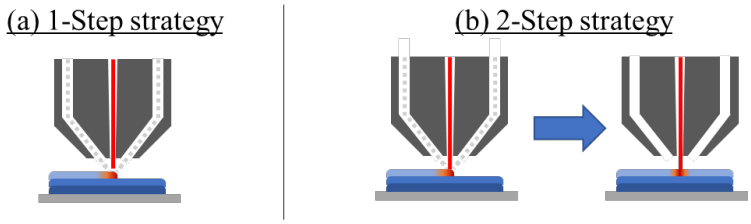

Fig. 1: Illustration of the two deposition strategies used (a): 1-step strategy and (b): 2-step strategy, with a re-melting step

Each single-track sample was made 3 consecutive times to assess the repeatability of the process. In order to analyze the composition of the powder exiting the printhead, powder was deposited without turning on the laser on steel substrate covered with glue, which will thereafter be referred to as “Sticky Bands”. This was made to retrieve a single layer of powder particle and avoid errors in composition analysis linked with density-based stratification of the various elements.

The printed samples were then cut and polished using SiC abrasive papers and diamond suspensions. The cross-sections were observed using a Zeiss EVO-15 scanning electron microscope (SEM) equipped with an Energy Dispersive X-Ray (EDX) for composition analysis.

Results

The results of the EDX analysis of the powders retrieved on three of the sticky bands is visible on Fig. 2.

The three bands, referred as S1, S2 and S3, where exposed to the powder flow under the same conditions at various moments of the sample manufacturing campaign. For each band, a minimum of 5 measurements was conducted. It appears that the composition of the retrieved powders strongly deviates from the expected one, and changes from one sticky band to the other. The mean deviation for one band remains low (>5%atm, except for the Ti on S1).

Regarding the SEM observations of the printed samples, the samples can be divided in two categories depending on whether or not they were subjected to a second re-melting laser-pass. A typical sectional view of a single-pass sample is visible on Fig. 3(a).

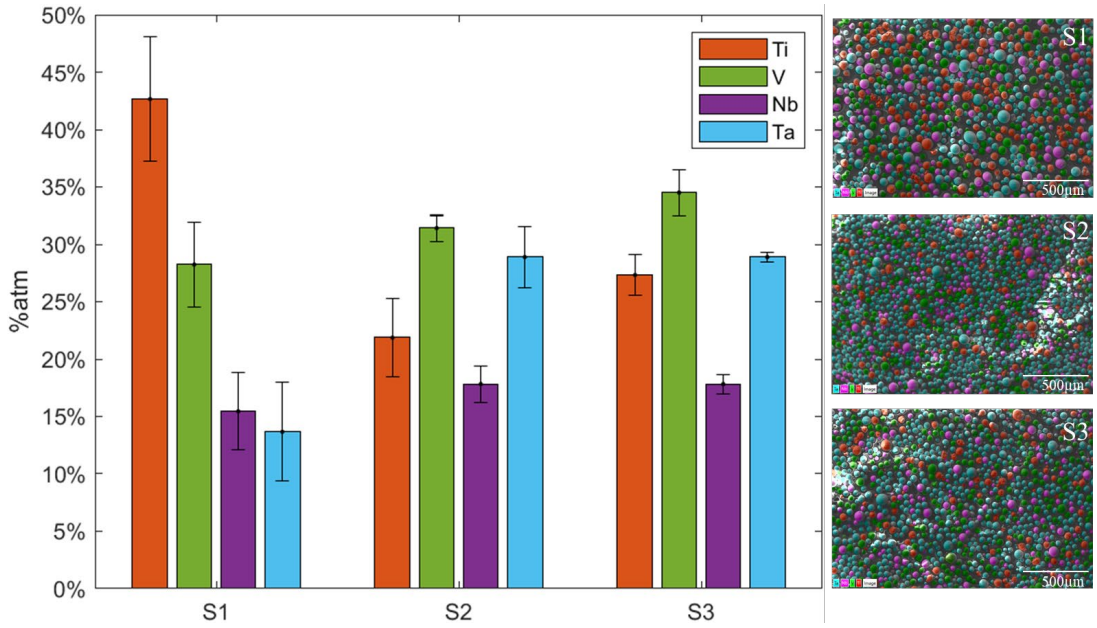

Fig. 2: Average composition of the powder retrieved on the sticky bands and associated mean deviation in the form of error bars, with corresponding examples of EDX mapping superimposed on SEM imageries.

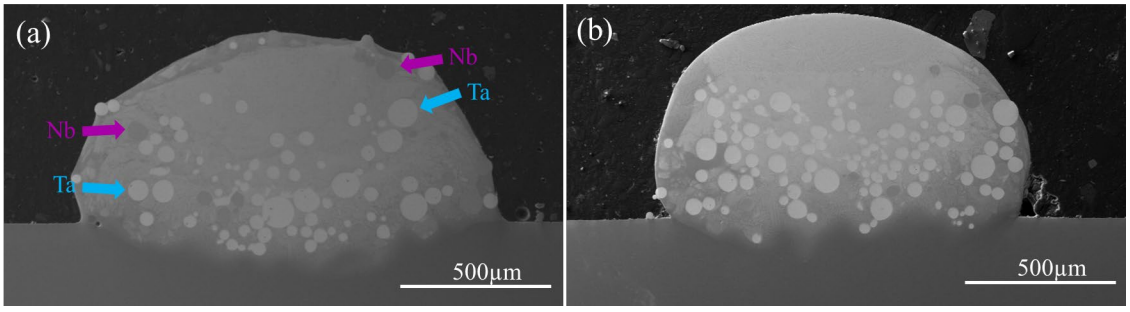

Fig. 3: SEM imaging of typical sectional views of (a) a single-pass sample printed with a P=500W, V=600mm/min and $\dot{m}$=7.3g/min and (b) a double-pass sample printed with the same parameters for the deposition steps and P=500W and V=400mm/min for the re-melting pass.

The first thing visible is the large amount of non-melted Ta particles (white particles, highlighted by blue arrows), and of Nb particles (dark particles, highlighted by purple arrows) in lesser proportions, whose presence can be explained by their extremely high melting point (T_{Ta}=3020°C and T_{Nb}=2477°C). Moreover, a large fraction of the single-pass samples exhibits a Ti-rich outer edge (darker edge on Fig. 3(a)). This partitioning of the elements is proof that the

inner part of the sample cooled first, leading to a partial segregation of the low-melting temperature Ti in said edges.

A typical sectional view of a double-pass sample is visible on Fig. 3(b). This sample also exhibits a large concentration of non-melted Ta particles. However, the upper fraction of the sample's cross section appears to be homogeneous. These homogeneous areas have a depth between 200 and 250µm.

Typical high-magnification EDX composition maps can be seen on Fig. 4. For all samples, a dendritic microstructure can be observed. The dendrites are Ta-rich, whereas the inter-dendrites are mostly Ti, V and Nb-rich. This is coherent with the melting points of the various elements, and confirms that, even though pure Ta particle can be seen, a fraction of it was indeed melted.

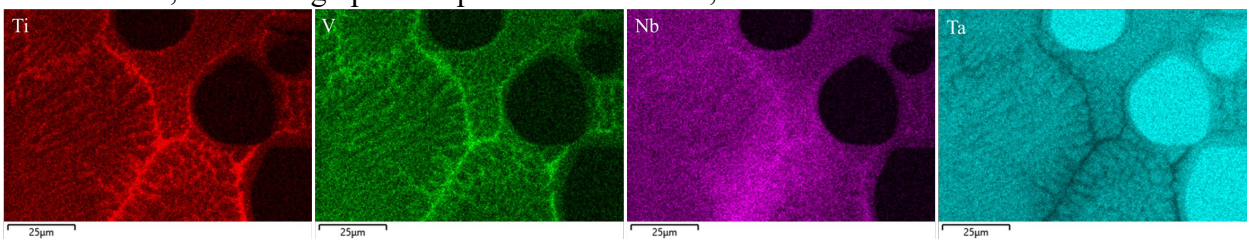

Fig. 4: x1000 Magnification EDX mapping of the various element's concentrations. These maps where acquired on a single-pass sample manufactured with P=500W and V=700mm/min

Nb concentration follows a peculiar behaviour compared to the other elements. Even though it appears to be concentrated in the inter-dendrites, the segregation does not appear as severe as it is for V and Ti. This hints towards a diffusion of Nb in the Ta-rich dendrites during the solidification process.

The composition of the single-tracks samples was analysed, and the average concentrations of each elements can be seen in Table 2.

Table 2: Average concentration of each elements in the single-track samples and corresponding standard deviation

	Ti	V	Nb	Ta
Average concentration (at.%)	28.0	11.9	14.9	45.2
Standard Deviation (at.%)	11.3	1.7	4.3	8.8

It appears that the composition of the samples strongly deviates from the expected equimolar one. V and Nb are underrepresented, whereas Ta is over-represented. The average Ti concentration is close to the expected one, but is highly variable from one sample to the next. This is most likely due to random levels of chemical contaminations from the substrates. This can be confirmed by analysing the concentration evolution of the various elements on the different layers of the wall-type samples.

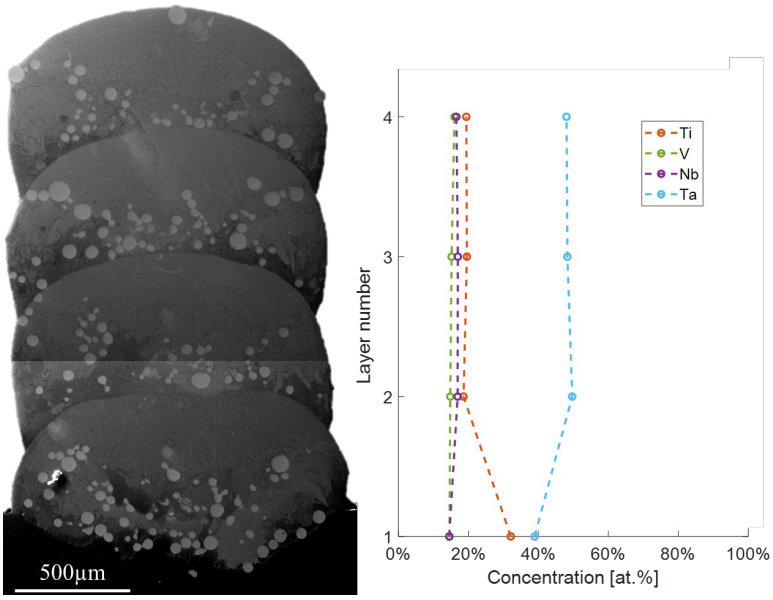

Fig. 5: Sectional view of a wall-type sample printed with the dual-pass method (P=500W, V=400mm/min and $\dot{m}$=3.5g/min for the deposition step, and P=500W and V=400mm/min for the re-melting step), and average concentration evolution of the various elements for the different layers for all wall type samples.

As it can be seen on Fig. 5, the average Ti concentration drops significantly between the first and second layer. The composition then remains stable along the sample's height. Moreover, as shown on Fig. 5, Ta particles can also be found in the wall structures. For the dual-pass samples, the top part of each layer is homogeneous, leading to high concentration of Ta particles at the interface between layers. Moreover, these walls structures are free of cracks and porosities.
The dimensions of the single-track samples were measured through image analysis. Fig. 6 shows the evolution of the samples' heights as a function of the deposition speed, regardless of laser power.

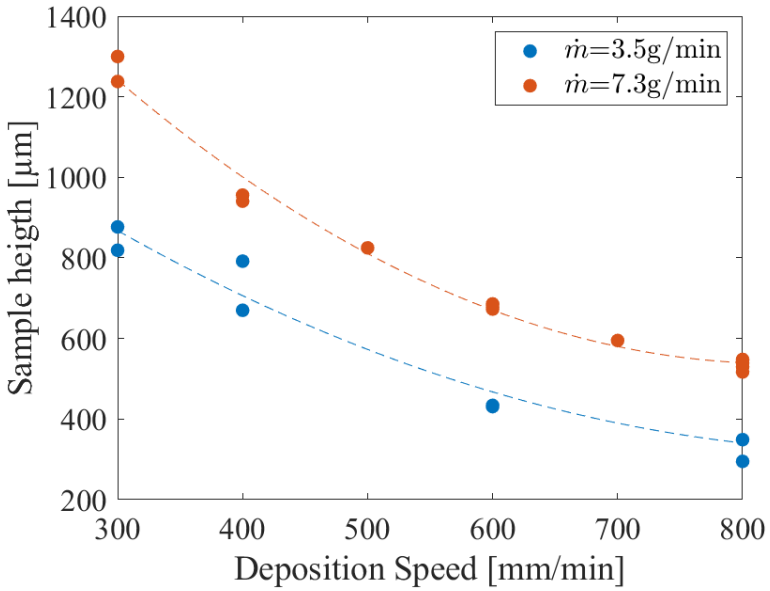

Fig. 6: Sample height of the single-track samples as a function of deposition speed for various powder mass flow rate, regardless of the laser power

It appears that a direct correlation exists between a sample's height and the deposition speed and powder mass flow with which it was deposited.

Discussion

The current main problematic is the high concentration of Ta particles in the samples, due to their high melting temperature. As the machine available for this study is only equipped with a 500W laser, the only way to increase the energy input is to reduce the deposition speed. However, doing so with a single-pass strategy means that more powder will be deposited, negating the benefice of the increased energy output.

Upon analysing the depth of the area homogenized by the re-melting step, one can notice that said depth remains fairly consistent from one sample to the next.

This, combined with the sample's height trend identified previously (Fig. 6), tends to show that the optimal method to achieve a complete melting of the matter is to use a high deposition speed and/or a low powder mass flowrate to obtain slim seams. This, combined with a re-melting pass, could ensure that a large fraction of the seam is homogenised, as illustrated on Fig. 7.

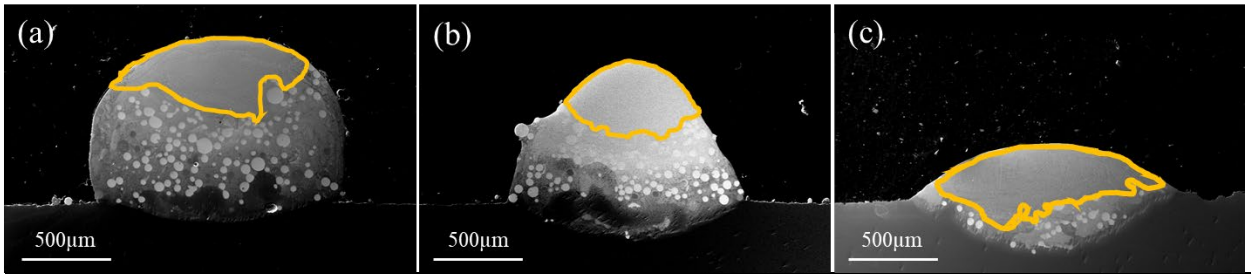

Deposition Parameters		
P=500W V=400mm/min $\dot{m}$=7.3g/min	P=500W V=400mm/min $\dot{m}$=3.5g/min	P=500W V=800mm/min $\dot{m}$=3.5g/min

Fig. 7: Cross section of 3 single track double-pass samples manufactured with the same re-melting parameters (P=500W and V=400mm/min) and different deposition parameters. The homogenised part of the cross-section is highlighted in yellow.

Another current issue lies in the control of the composition of the powder feed. The analysis of the powder retrieved on the sticky bands shows that powder composition does not evolve much when measured on a single band, meaning that instantaneous variation in the composition are low. However, the composition differences between different bands are very large. This goes to show that the powder mixture in the printer's hopper is imperfect. Multiple root cause can be identified. First, the strong density difference between the various powders can lead to a de-mixing of the powders over time. Moreover, the manual mixing might not be enough to fully homogenise the mixture, even though only a small quantity of powders was mixed at a given time. Better mixing procedures, compatible with the high oxidation rate of pure elemental powders, needs to be put in place.

Even if the composition of the powder feed is variable, a clear tendency appears in the composition of the samples. The chemical analysis of the wall-type samples proves that the Ta has a much higher deposition efficiency compared to the other elements (Fig. 5). This goes against what can be seen in the literature regarding the manufacturing of RHEA through LMD, where the elements with the highest melting point are usually the ones with the lowest deposition efficiency due to them bouncing off the melt pool [9], [11], [12]. This phenomenon can be explained by the large fraction of Ta particles of smaller diameter, the later having a higher chance of sticking to the melt pool.

Conclusions

From the present study, the following conclusions can be drawn:

1/ Manufacturing the NbTaTiV alloy by LMD with a 500W laser leads to the formation of a beads containing a large concentration of non-melted Ta and Nb powders, due to their high melting temperature.

2/Using a dual-pass deposition strategy (deposition followed by re-melting) creates a homogenized zone in the upper part of the bead's cross-section. Reducing the bead's height by increasing the deposition speed and reducing the powder mass flowrate can allow to fully homogenize the cross-section.

3/ The samples all present a dendritic microstructure with Ta-rich dendrites. The samples all present a high Ta concentration, due to a higher deposition efficiency of Ta particles.

4/ The powder composition appears to be variable over time. This variation can be attributed to an imperfect mixing of the powder in the hoppers.

References

[1] J.-W. Yeh *et al.*, "Nanostructured High-Entropy Alloys with Multiple Principal Elements: Novel Alloy Design Concepts and Outcomes," *Advanced Engineering Materials*, vol. 6, no. 5, pp. 299–303, 2004. https://doi.org/10.1002/adem.200300567

[2] B. Cantor, I. T. H. Chang, P. Knight, and A. J. B. Vincent, "Microstructural development in equiatomic multicomponent alloys," *Materials Science and Engineering: A*, vol. 375–377, pp. 213–218, Jul. 2004. https://doi.org/10.1016/j.msea.2003.10.257

[3] O. N. Senkov, G. B. Wilks, D. B. Miracle, C. P. Chuang, and P. K. Liaw, "Refractory high-entropy alloys," *Intermetallics*, vol. 18, no. 9, pp. 1758–1765, Sep. 2010. https://doi.org/10.1016/j.intermet.2010.05.014

[4] O. N. Senkov, G. B. Wilks, J. M. Scott, and D. B. Miracle, "Mechanical properties of Nb25Mo25Ta25W25 and V20Nb20Mo20Ta20W20 refractory high entropy alloys," *Intermetallics*, vol. 19, no. 5, pp. 698–706, May 2011. https://doi.org/10.1016/j.intermet.2011.01.004

[5] R. Feng *et al.*, "Superior High-Temperature Strength in a Supersaturated Refractory High-Entropy Alloy," *Advanced Materials*, vol. 33, no. 48, p. 2102401, 2021. https://doi.org/10.1002/adma.202102401

[6] H. Dobbelstein, M. Thiele, E. L. Gurevich, E. P. George, and A. Ostendorf, "Direct Metal Deposition of Refractory High Entropy Alloy MoNbTaW," *Physics Procedia*, vol. 83, pp. 624–633, Jan. 2016. https://doi.org/10.1016/j.phpro.2016.08.065

[7] J. P. Couzinié *et al.*, "Microstructure of a near-equimolar refractory high-entropy alloy," *Materials Letters*, vol. 126, pp. 285–287, Jul. 2014. https://doi.org/10.1016/j.matlet.2014.04.062

[8] C. Lee *et al.*, "Lattice distortion in a strong and ductile refractory high-entropy alloy," *Acta Materialia*, vol. 160, pp. 158–172, Nov. 2018. https://doi.org/10.1016/j.actamat.2018.08.053

[9] M. A. Melia *et al.*, "High-throughput additive manufacturing and characterization of refractory high entropy alloys," *Applied Materials Today*, vol. 19, p. 100560, Jun. 2020. https://doi.org/10.1016/j.apmt.2020.100560

[10] H. Dobbelstein, E. L. Gurevich, E. P. George, A. Ostendorf, and G. Laplanche, "Laser metal deposition of compositionally graded TiZrNbTa refractory high-entropy alloys using elemental powder blends," *Additive Manufacturing*, vol. 25, pp. 252–262, Jan. 2019. https://doi.org/10.1016/j.addma.2018.10.042

[11] H. Dobbelstein, E. L. Gurevich, E. P. George, A. Ostendorf, and G. Laplanche, "Laser metal deposition of a refractory TiZrNbHfTa high-entropy alloy," *Additive Manufacturing*, vol. 24, pp. 386–390, Dec. 2018. https://doi.org/10.1016/j.addma.2018.10.008

[12] H. Dobbelstein, E. P. George, E. L. Gurevich, A. Kostka, A. Ostendorf, and G. Laplanche, "Laser metal deposition of refractory high-entropy alloys for high-throughput synthesis and structure-property characterization," *Int. J. Extrem. Manuf.*, vol. 3, no. 1, p. 015201, Dec. 2020. https://doi.org/10.1088/2631-7990/abcca8